

Infrared and ultraviolet properties of the Landau gauge quark propagator

Patrick O. Bowman^{a*}, Urs M. Heller^b, Derek B. Leinweber^a, Anthony G. Williams^a and Jianbo Zhang^a

^aDepartment of Physics and CSSM, University of Adelaide, Australia 5005

^bAmerican Physical Society, One Research Road, Box 9000, Ridge, NY 11961-9000

We present a current summary of a program to study the quark propagator using lattice QCD. We use the Overlap and “Asqtad” quark actions on a number of lattice ensembles to assess systematic errors. We comment on the place of this work amongst studies of QCD Green’s functions in other formulations. A preliminary calculation of the running quark mass is presented.

1. INTRODUCTION

The quark propagator is a building block of Quantum Chromodynamics and has been studied in numerous formulations [1,2,3]. The lattice regularisation provides a method for a full non-perturbative calculation from first principles. In the infrared, the quark propagator displays dynamical mass generation, but in the ultraviolet it takes its perturbative, running form.

By computing the quark propagator on the lattice we can connect with perturbation theory and with many models. We can also contribute to our understanding of the inner workings of the lattice simulations themselves. It has been seen, however, that detailed lattice studies of the quark propagator require sophisticated actions [4,5,6,7,8,9].

We present some results for the quark propagator in Landau gauge from a variety of lattice spacings, two different physical volumes and two different quark actions. Specifically we use an improved Staggered action, “Asqtad,” [10] and the Overlap quark action. Results from Asqtad and Overlap actions are in good agreement. We will compare our results to some model calculations and compare our chiral extrapolation with recent Dyson–Schwinger equation predictions. Not only do we see stable infrared results, but the ultraviolet data is good enough for us to attempt estimates of the chiral condensate and the running quark mass. A much more detailed presentation

can be found in Ref. [11]. The quark propagator was also studied in Laplacian gauge in Ref. [6].

2. THE LATTICE QUARK PROPAGATOR

In the (Euclidean) continuum, Lorentz invariance allows us to decompose the full quark propagator into Dirac vector and scalar pieces

$$S(p^2; m) = \frac{Z(p^2)}{i\gamma \cdot p + M(p^2)}. \quad (1)$$

Asymptotic freedom means that at large momentum transfer, $p^2 \rightarrow \infty$, the quark propagator approaches its free form,

$$S(p^2; m) \rightarrow \frac{1}{i\gamma \cdot p + m}, \quad (2)$$

where m is a current quark mass. On the lattice in the free case ($U_\mu(x) = 1$), the quark propagator takes the form,

$$S(p_\mu; m) = \frac{1}{i\gamma \cdot q(p_\mu) + m}, \quad (3)$$

where the function $q_\mu(p_\mu)$ depends on the quark action. For the Asqtad action it is [6],

$$q_\mu = \sin(p_\mu) \left[1 + \frac{1}{6} \sin^2(p_\mu) \right], \quad (4)$$

and for the Overlap action it is [8],

$$q_\mu = 2m_w \frac{\tilde{q}_\mu \{A + \sqrt{\tilde{q}^2 + A^2}\}}{\tilde{q}^2}, \quad (5)$$

*Presented by POB.

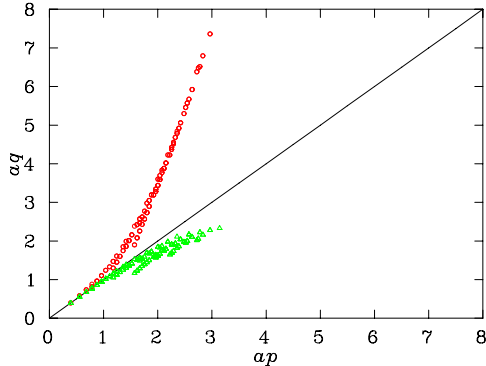


Figure 1. Tree-level behaviour: q vs. p for the Overlap (top curve) and Asqtad (bottom curve) quark actions. This is the inverse of the propagator for a massless quark. The diagonal line is the continuum case.

where

$$\begin{aligned}
 A &= -m_w + \frac{\hat{k}^2}{2} \\
 \tilde{q}_\mu &= \sin(p_\mu) \\
 \hat{k}_\mu &= 2 \sin(p_\mu/2),
 \end{aligned}$$

and m_w is the regulator mass. These functions are plotted in Fig. 1

The difference between Eq. (2) and Eq. (3) is a pure lattice artefact. For the Dirac vector piece this can be trivially corrected for by considering it to be a function not of p_μ , but of q_μ . This only affects the ultraviolet behaviour of Z , and asymptotic freedom means that we may hope that this correction will persist in the interacting case. This choice of “kinematical momentum” has been seen to be efficacious in the removal of hypercubic artefacts [6] and the philosophy is the same as that pursued with great success in studies of the gluon propagator [12]. Tree-level correction does not prescribe such a procedure for the Dirac scalar piece, M , so we shall adopt an empirical approach.

Table 1

Simulation parameters

Action	β	a_σ (fm)	$L^3 \times T$
Asqtad	4.38	0.167	$16^3 \times 32$
Asqtad	4.60	0.124	$12^3 \times 24$
Asqtad	4.60	0.124	$16^3 \times 32$
Overlap	4.286	0.190	$8^3 \times 16$
Overlap	4.60	0.124	$12^3 \times 24$
Overlap	4.80	0.093	$16^3 \times 32$

3. RESULTS

3.1. Lattice artefacts

The simulation parameters are given in Table 1. In all cases an $\mathcal{O}(a^2)$ Symanzik improved gluon action was used. The propagators were rotated to $\mathcal{O}(a^2)$ -improved Landau gauge [13] by standard methods.

As we have both Overlap and Asqtad results for one set of lattices we can make a direct comparison. This is shown in Fig. 2 for one choice of comparable quark masses. Z is shown as a function of q – chosen appropriately for each action – and there is complete agreement, within errors. The Asqtad action has notably better rotational symmetry, presumably reflecting the removal of $\mathcal{O}(a^2)$ errors. Recently, one group has attempted to correct the poor rotational symmetry of the Overlap action by extrapolating in the hypercubic artefacts [14]. The quark mass function for the Asqtad action is shown as a function of q , which has been seen to produce slightly better results [7], but we use the standard lattice momentum, p for the Overlap action. This choice produces the best agreement between the two actions.

Figure 3 shows the Asqtad quark propagator on two different size lattices with the same lattice spacing. The smaller lattice has a spatial length of about 1.5 fm, the larger about 2.0 fm. The mass functions lie on top of each other, indicating that finite volume effects are small, if present. For Z however, there is a clear difference in the low momentum region. Infrared suppression of Z is a long-standing prediction of Dyson–Schwinger equation studies and the larger lattice results are in good agreement with recent DSE results [15],

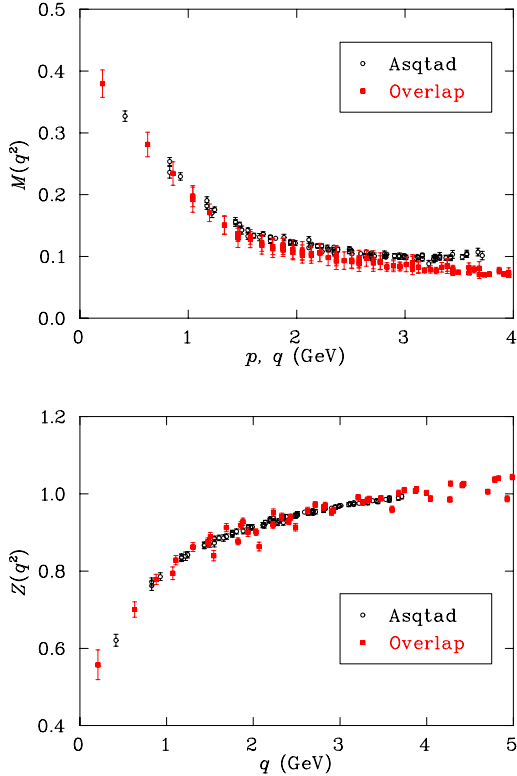


Figure 2. Comparison of the actions: Quark mass function (top) and Z function (bottom) for mass $m \simeq 80$ MeV at $\beta = 4.60$. These calculations were performed on a $12^3 \times 24$ lattice.

but at least some of the suppression may be due to the finite volume.

As we have the Overlap quark propagator at three lattice spacings we can examine its scaling behaviour. This is shown in Fig. 4. For both functions we see good consistency across these lattice spacings. Once again, we have plotted Z against q and M against p . This gives the best agreement between results at different lattice spacings. The violation of rotational symmetry seen in Z – quite strong on the coarsest lattice – becomes smaller with the lattice spacing, but the overall form is stable. The infrared behaviour of the mass function is almost unaffected by the change in lattice spacing, but the ultraviolet shows some (not unexpected) sensitivity.

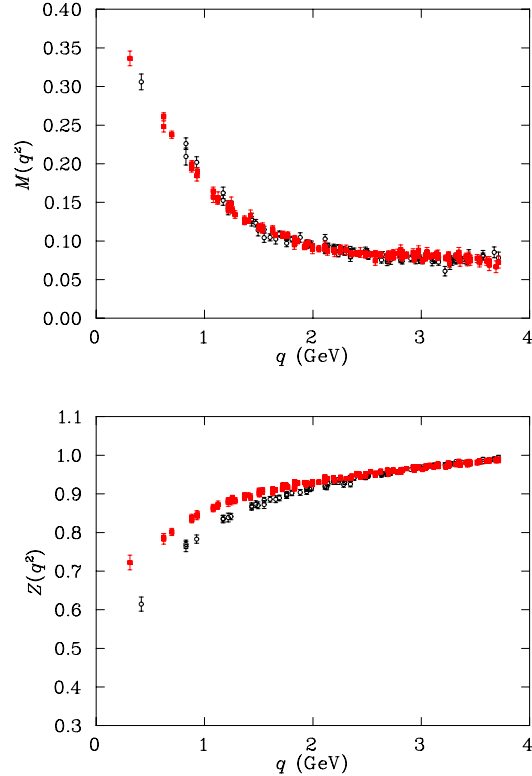


Figure 3. Finite volume effects: Asqtad quark mass function (top) and Z function (bottom) for mass $m \simeq 57$ MeV at $\beta = 4.60$. Comparison on $12^3 \times 24$ lattice (open circles) and 16×32 lattice (solid squares).

The quark propagator is, of course, a function of the bare quark mass, and this dependence is illustrated in Fig. 5. For the Z function we show results for three quark masses from the Asqtad action, and indeed some mass dependence is observed in the infrared. The heaviest quark has about four times the mass of the lightest one, so this dependence is rather weak. We expect the ultraviolet to be insensitive to the quark mass and this is in fact observed. The ultraviolet tail of the mass function is proportional to the bare quark mass and this is observed in Fig. 5 using the Overlap action. As the mass increases the infrared enhancement becomes less significant. It has already been remarked elsewhere [7] that for

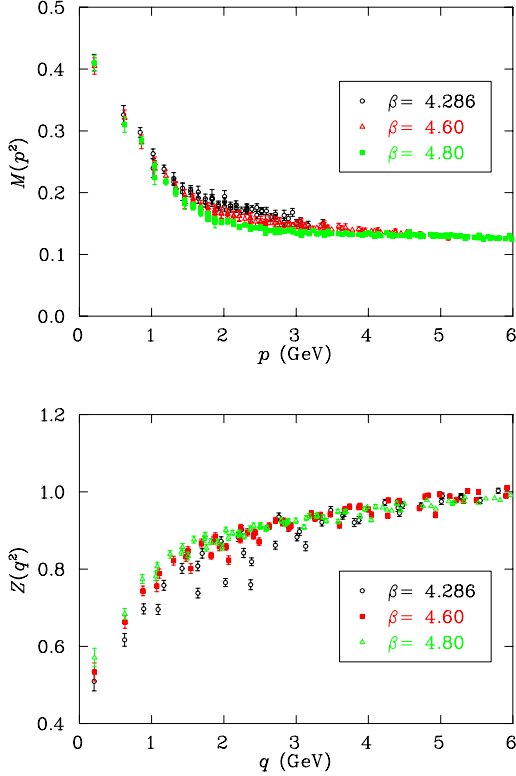


Figure 4. Scaling: Quark mass (top) and Z (bottom) for the Overlap action at three lattice spacings. Bare quark mass $m \simeq 106$ MeV. Z is shown as a function of q while M is a function of p . This is seen to provide the best agreement between results on different lattice spacings.

small quark masses the infrared part of the mass function is insensitive to the quark mass, but at around the strange quark mass the shape of the mass starts to change. In the non-relativistic limit $M(p^2)$ would be a constant.

3.2. Comparison with other methods

We extrapolate the quark mass function to the chiral limit using a quadratic fit. One reason for this is that it is a convenient quantity to compare with other calculations. In Ref. [3] the authors suggested a novel form of the quark mass function which actually vanishes at zero four-momentum.

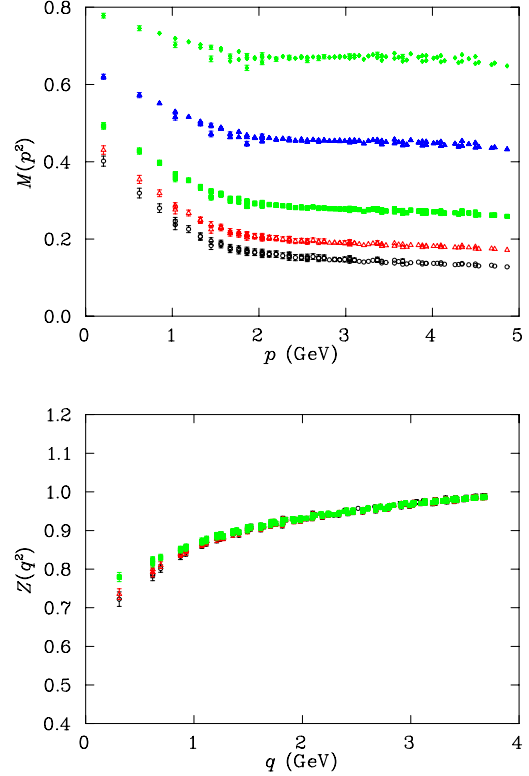


Figure 5. Mass dependence: Asqtad Z function at $\beta = 4.60$, $16^3 \times 32$, for bare quark masses $m \simeq 57$, 115 and 229 MeV. There is some weak mass dependence in the infrared. Overlap mass function at $\beta = 4.60$, $12^3 \times 24$, for bare quark masses $m \simeq 106 - 531$ MeV. For large momentum, $M(p^2)$ is proportional to the quark mass and as the mass increases, $M(p^2)$ becomes flatter.

The ansatz

$$M(q^2) = \frac{1 - \sqrt{1 - q^2 Q^2(q^2)}}{Q(q^2)}, \quad (6)$$

where

$$Q(q^2) = \frac{-\langle \bar{\psi} \psi \rangle}{2N_c} \frac{16\pi^2}{\lambda^4} e^{-q^2/\lambda^2}, \quad (7)$$

based on the Constrained Instanton Model and QCD sum rules with non-local condensates, is one of the curves shown in Fig. 6. This form is not favoured by the lattice data. It is fascinating that such a form should be consistent

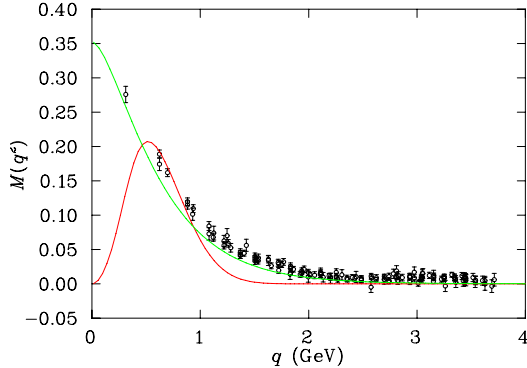


Figure 6. Comparison with two models: The mass function that vanishes at zero four-momentum is from a model of Dorokhov and Broniowski [3], the other is from an instanton calculation by Diakonov [2].

with the phenomenological constraints discussed in Ref. [3] and demonstrates the utility of first-principles calculations.

Figure 6 also shows a regular instanton model calculation from Ref. [2]. There the quark mass function takes the form

$$\begin{aligned}
 M(q) &= M(0)F^2(z) & (8) \\
 F(z) &= 2z \left(I_0(z)K_1(z) - I_1(z)K_0(z) \right. \\
 &\quad \left. - I_1(z) \frac{K_1(z)}{z} \right) \\
 z &= q \frac{\rho}{2}
 \end{aligned}$$

where the I 's and K 's are the modified Bessel functions. The parameters $M(0) = 350$ MeV and $\rho^{-1} = 600$ MeV are derived from the standard values of the instanton ensemble. This two parameter form has a good correspondence with the lattice data.

The interaction between lattice and DSE studies has been particularly active recently. See Refs. [15,16,17,18] for a few examples. Amongst other things, this is providing valuable insight about the validity of various DSE truncation schemes. In return, DSE calculations can be done at quark masses and momenta difficult to access on the lattice and can also provide information

on the time-like region.

In Ref. [15] there is a comparison of the lattice quark mass function at various quark masses with a form derived from the Dyson–Schwinger equation. The DSE describes the lattice data well at finite quark mass, but there is some difference in the chiral limit. In particular the DSE solution changes more rapidly with momentum around one GeV. This suggests some non-linear behaviour at intermediate momenta and small quark masses, not captured by our simple extrapolation. While such behaviour is certainly not surprising, it is also not well understood.

4. ASYMPTOTIC BEHAVIOUR

As we have already remarked, although the quark propagator is gauge dependent, and hence not observable, certain gauge invariant quantities can be extracted from it directly. In the continuum, the quark mass function has the asymptotic form [1],

$$\begin{aligned}
 M(q^2) &\underset{q^2 \rightarrow \infty}{=} \frac{c}{q^2} [\ln(q^2/\Lambda_{\text{QCD}}^2)]^{d_M-1} \\
 &\quad + \frac{\hat{m}}{[\ln(q^2/\Lambda_{\text{QCD}}^2)]^{d_M}} \quad (9)
 \end{aligned}$$

where \hat{m} is the RGI (renormalisation group invariant) mass and the anomalous dimension of the quark mass is $d_M = 12/(33 - 2N_f)$ for N_f quark flavours (zero here). In this form the fact that the mass function is independent of the choice of renormalisation point is manifest. The first term in Eq. (9) is of nonperturbative origin and, in the chiral limit, a non-zero value for c indicates the spontaneous breaking of chiral symmetry. In this case it is related to the usual chiral condensate by

$$c \simeq -\frac{4\pi^2 d_M}{3} \frac{\langle \bar{\psi}\psi \rangle}{[\ln(\mu^2/\Lambda_{\text{QCD}}^2)]^{d_M}}, \quad (10)$$

where μ^2 is a choice of renormalisation point. The second term in Eq. (9) comes from perturbation theory (one-loop) and breaks chiral symmetry explicitly. The RGI quark mass in Eq. (9) can be replaced by the running quark mass,

$$\hat{m} = m(\mu^2) [\ln(\mu^2/\Lambda_{\text{QCD}}^2)]^{d_M}. \quad (11)$$

Table 2

Results for the fit to Eq. (9). The fit region corresponds to 1.9-2.9 GeV, which includes 51 data points, and was chosen to minimise the χ^2/dof . In the chiral limit this gives a value for the condensate of $(-\langle\bar{\psi}\psi\rangle)^{1/3} = 274(24)$ MeV at the renormalisation point $\mu = 2$ GeV.

am	a^3c	\hat{m} (MeV)	$\chi^2 / \text{d.o.f.}$
0	0.018(6)	0	0.52
0.012	0.019(3)	28(2)	0.57
0.018	0.014(12)	44(5)	0.54
0.024	0.0096(47)	59(3)	0.52
0.036	0.0026(104)	90(5)	0.49
0.048	0.086(3)	137(4)	0.46
0.072	0.130(3)	204(5)	0.40
0.108	0.190(3)	300(5)	0.31
0.144	0.251(5)	397(8)	0.25

Table 2 summarizes results for a fit of Eq. (9) to our lattice results.

Having fit the asymptotic form to the quark mass function we should also be able to calculate the quark mass, but there is one piece of information missing from Table 2. The effect of the bare quark mass on physical quantities is theory dependent; we have no *a priori* knowledge of where the physical point lies. We can match a physical quantity to its real world value and thus extract the relevant bare mass for that particular action, with those particular lattice parameters. In this case we choose the Asqtad quark action on the $16^3 \times 32$ lattice at $\beta = 4.60$ and set the “physical” bare quark mass by extrapolation to the physical pion mass.

We fit the five lowest π masses to the form

$$am_\pi = \sqrt{a^2 B m}, \quad (12)$$

the lowest order result from chiral perturbation theory. For the higher masses, the data deviates from this form due to the contribution from higher order terms; in the heavy quark limit $m_\pi \propto m$. The U(1) chiral symmetry of staggered quarks ensures that there is no additive mass renormalisation. To find the physical point we find the bare mass corresponding to $m_\pi = 140$ MeV for each jackknife bin and get $am = 0.00215(1)$. Then we

fit the lowest four RGI masses in Table 2 to the form

$$a\hat{m} = Aam \quad (13)$$

and find $A = 1.57(16)$. Putting these together we get

$$\hat{m} = 5.3(6)\text{MeV}.$$

The RGI quark mass in Eq. (9) is related to the running quark mass through Eq. (11). Thus by choosing the renormalisation point $\mu = 2$ GeV and inserting $\Lambda_{\text{QCD}}^{\overline{\text{MS}}} = 239$ MeV, we get

$$m(\mu = 2 \text{ GeV})^{\overline{\text{MS}}} = 3.1(4)\text{MeV},$$

or with $\Lambda_{\text{QCD}}^{\overline{\text{MOM}}} = 691$ MeV,

$$m(\mu = 2 \text{ GeV})^{\overline{\text{MOM}}} = 4.0(5)\text{MeV}.$$

This result compares favourably with the Particle Data Group’s number for the average of the up and down quark masses [19],

$$\overline{m}(\mu = 2 \text{ GeV})^{\overline{\text{MS}}} = 2.5 - 5.5\text{MeV}.$$

The curious behaviour of the condensate term at small masses is easily explained. The asymptotic behaviour of the quark mass function quickly becomes dominated by the explicit chiral symmetry breaking mass; at the same time, large fluctuations make the mass function relatively noisy at these masses. Together, that means that sensitivity of the fit to the first term in Eq. (9) is lost. At larger masses, the signal becomes cleaner and statistical errors shrink, restoring stability to the fits. One way of countering this effect would be to fix ac for each light mass to some reasonable value given the chiral and heavy quark values. The difference to the end result would be small, but a future study should consider such systematics.

This calculation is, of course, quenched. There are also systematic errors associated with the two extrapolations. Using other observables to set the scale – such as the ρ and nucleon masses, possibly supported by the appropriate finite-range regulated [20,21] staggered chiral perturbation theory

[22,23] – would help us understand the systematic uncertainty associated with the extrapolation. Such an approach could also provide a handle on the uncertainty associated with quenching. Finally, we should realise that this is a rather audacious approach: we are exploiting ultraviolet physics on a relatively coarse lattice. It is very encouraging, however, that we are able to get such a promising result with such modest resources. The choices of improved quark and gauge actions are essential to this.

5. CONCLUSIONS

A comprehensive understanding of the quenched quark propagator in Landau gauge is now in place. Overlap and Improved Staggered actions produce propagators that are well behaved over a wide range of momenta. Despite this, more points in the deep infrared are required to pin down precisely the behaviour near zero four-momentum. Also, the role of finite volume effects in the Z function at small quark masses needs further investigation. Calculations using dynamical configurations are underway.

ACKNOWLEDGMENTS

The authors would like to thank the organisers of the Lattice Hadron Physics workshop (Cairns, 2003) for a great workshop.

REFERENCES

1. C.D. Roberts and A.G. Williams, Prog. Part. Nucl. Phys. **33**, (1994) 477.
2. D. Diakonov, hep-ph/0212026.
3. A.E. Dorokhov and W. Broniowski, Phys. Rev. D **65**, (2002) 094007.
4. J-I. Skullerud and A.G. Williams, Phys. Rev. D **63**, (2001) 054508.
5. J. Skullerud *et al.*, Phys. Rev. D **64**, (2001) 074508.
6. P.O. Bowman, U.M. Heller and A.G. Williams, Phys. Rev. D **66**, (2002) 014505.
7. P.O. Bowman, U.M. Heller, D.B. Leinweber and A.G. Williams, hep-lat/0209129.
8. F.D.R. Bonnet, P.O. Bowman, D.B. Leinweber, A.G. Williams and J. Zhang, Phys. Rev. D **65**, (2002) 114503.
9. J.B. Zhang, F.D.R. Bonnet, P.O. Bowman, D.B. Leinweber and A.G. Williams, hep-lat/0301018.
10. K. Orginos, D. Toussaint and R.L. Sugar, Phys. Rev. D **60**, (1999) 054503.
11. *The Quark Propagator and its Physical Implications*, in A. Kalloniatis *et al.* (eds.), Lattice Hadron Physics, Springer-Verlag, to be published.
12. F.D.R. Bonnet, P.O. Bowman, D.B. Leinweber, A.G. Williams and J.M. Zanotti, Phys. Rev. D **64**, (2001) 034501.
13. F. D. R. Bonnet, P. O. Bowman, D. B. Leinweber, A. G. Williams and D. G. Richards, Austral. J. Phys. **52** (1999) 939 [arXiv:hep-lat/9905006].
14. P. Boucaud *et al.*, hep-lat/0307026.
15. M.S. Bhagwat, M.A. Pichowsky, C.D. Roberts and P.C. Tandy, nucl-th/0304003.
16. M. Oettel and R. Alkofer, Eur. Phys. J. **A 16**, (2003) 95.
17. H. Iida, M. Oka and H. Suganuma, hep-lat/0309338.
18. R. Alkofer, W. Detmold, C.S. Fischer and P. Maris, hep-ph/0309077.
19. K. Hagiwara *et al.*, Phys. Rev. D **66**, (2002) 010001.
20. R. D. Young, D. B. Leinweber and A. W. Thomas, Prog. Part. Nucl. Phys. **50** (2003) 399 [arXiv:hep-lat/0212031].
21. D. B. Leinweber, A. W. Thomas and R. D. Young, arXiv:hep-lat/0302020.
22. C. Aubin and C. Bernard, Phys. Rev. D **68** (2003) 034014 [arXiv:hep-lat/0304014].
23. C. Aubin and C. Bernard, Phys. Rev. D **68** (2003) 074011 [arXiv:hep-lat/0306026].